Ground Motions from Three Recent Earthquakes in Western Alberta and Northeastern British Columbia and Their Implications for Induced-Seismicity Hazard in Eastern Regions

by Gail Atkinson, Karen Assatourians, Burns Cheadle, and Wes Greig

ABSTRACT

A key issue in the assessment of hazard due to induced seismicity from fluid injection activity is to determine the potential ground motions. Although wastewater disposal typically receives the most attention, hydraulic fracturing is increasingly recognized as a significant source of seismic hazard. We present an analysis of the ground motions from the three largest events of 2014 that occurred along the deformation front marking the western boundary of the stable Canadian craton: an **M** 4.0 and an **M** 4.2 near Fort St. John (FSJ), British Columbia, and an **M** 3.9 near Rocky Mountain House (RMH), Alberta. The two FSJ events were likely induced by hydraulic fracturing activities in the region. Although the cause of the RMH event remains unclear, it is of interest because it is of similar magnitude to the other events and had significant consequences to the public. The event triggered an automatic shutdown of a nearby gas plant and a subsequent precautionary flaring of gas, and several hundred people were without power for a prolonged period. We examine the ground motions and intensities for these events. We find that ground motions at frequencies up to about 2 Hz are in agreement with corresponding observations for similar-sized events in California and with the predictions of applicable empirical ground-motion prediction equations. However, high-frequency ground motions appear to be lower than those predicted, suggesting that these events may be associated with a low stress drop; we believe that this is likely a focal depth effect, which may be a mitigating factor that limits high-frequency ground motions from induced events.

Our preliminary findings suggest that moderate-induced events (**M** 4–5) may be damaging to nearby infrastructure, because the shallow focal depth may result in localized strong ground motions to which some infrastructure may be vulnerable; this is a particular concern in low-to-moderate seismicity regions, because seismic design measures for structures in these regions may be minimal. Our results highlight the importance of seismic monitoring in the immediate vicinity of fluid injection sites (both wastewater disposal and hydraulic fracturing) to accurately characterize injection-induced seismicity and ultimately mitigate the associated risk.

INTRODUCTION

An important contemporary issue for seismic-hazard assessment in eastern North America concerns the potential magnitudes and ground motions from events triggered by oil and gas activity. This paper summarizes the ground motions from three recent felt events of moment magnitude (**M**) ~4 in northeastern British Columbia and western Alberta, which occurred between 30 July 2014 and 9 August 2014 in low-to-moderate seismicity regions east of the Rocky Mountains deformation front. We focus in particular on the implications of these events for potential ground motions from events induced by hydraulic fracturing, as ground motions are key to the assessment of hazard from induced seismicity. This issue is of particular importance in resource-rich regions of low-to-moderate hazard, because infrastructure in these regions may not have been designed to withstand strong ground motions, due to the low likelihood of strong shaking from naturally occurring events. The addition of a new source of hazard fundamentally alters the probability of experiencing strong ground motions, and the assessment of the potential ground motions is, therefore, critical to the evaluation of hazard and risk. Because the three events occurred close to the deformation front, they might reasonably be considered as either eastern or western events. Recent studies have shown that eastern and western motions are very similar at distances less than 50 km for events of the same magnitude, except at high frequencies (> 5 Hz) (e.g., Hassani and Atkinson, 2015), so the distinction between eastern and western may not be critical. Moreover, there is also a potential difference in ground motions between induced and natural events that is likely related to focal depth and which may be a more significant factor

doi: 10.1785/0220140195

(e.g., Atkinson, 2015; Hough, 2014). Thus at this stage of our understanding, the motions from these events are of great interest, regardless of whether they are considered to be more nearly eastern or western in terms of their tectonic setting.

Most attention on induced-seismicity hazard to date has focused on events triggered by deep disposal of fluids, as this appears to be the most common induced-seismicity trigger, and has recently been associated with events as large as **M** 5.7 (Ellsworth, 2013; Keranen *et al.*, 2013; Sumy *et al.*, 2014). However, there is increasing awareness of the potential of hydraulic fracturing to induce significant seismicity. Moreover, the largest reported events of this type continue to grow in magnitude. As of 2012, empirical evidence suggested that hydraulic fracture treatments had limited potential to induce significant events, as the largest known event was an **M** 2.8 event near Blackpool, England (U.S. National Research Council, 2012). Subsequently, several larger events have been triggered by hydraulic fracturing. In 2011, a series of dozens of events was triggered by hydraulic fracture treatments that reactivated previously unknown faults near Horn River, northeastern British Columbia; the largest event of the sequence was **M** 3.6–3.8 (B.C. Oil and Gas Commission, 2012). The size of the triggered events at Horn River was thought to be very unusual until December 2013, when a new sequence of dozens of hydraulic-fracture-induced events of **M** ~ 3 was initiated in the Crooked Lake region of western Alberta (a few hundred kilometers west of Edmonton, Alberta) (Novakovic *et al.*, 2014; Atkinson *et al.*, 2015; for catalog information see www.inducedseismicity.ca; last accessed March 2015). Until very recently, the largest event of that sequence was of magnitude **M** 3.5; then, on 23 January 2015, an event of **M** > 4 (M_L 4.4) occurred (which we are currently analyzing).

In August 2014, a series of events was initiated by hydraulic fracturing in the Montney formation near Fort St. John (FSJ, eastern British Columbia), the largest of which was an **M** 4.2 event on 4 August 2014 (Fig. 1). This event was preceded by an **M** 4.0 event in the same location on 30 July 2014. The two FSJ events were recorded by a sparse seismographic network, at distances from 15 km to several hundred kilometers. By coincidence, an event of similar size (**M** 3.9) occurred a few hundred kilometers away, near Rocky Mountain House (RMH) in western Alberta, on 9 August 2014. The RMH event is not believed to be related to hydraulic fracturing. Its origin is unclear as of yet; it may be related to fluid injection or gas withdrawal, or it may be natural. Regardless of its cause, the RMH event is important because it was recorded by a denser network over a wide range of distances and is similar in magnitude to the hydraulic-fracture-induced events. The additional ground-motion information provided by the **M** 3.9 RMH event, when combined with the data from the FSJ events, enables a robust analysis of the ground-motion implications of these moderate events.

In this paper, we use the recordings from these three recent **M** ~ 4 events to examine the ground motions and their attenuation with distance. The **M** 4.2 event is of particular interest, as it is the largest hydraulic fracturing related event to have been triggered in the world to date, to our knowledge. (As of 23 January 2015, this magnitude may have been exceeded by an M_L 4.4 event near Crooked Lake; the moment magnitude of the Crooked Lake event is currently under investigation.)

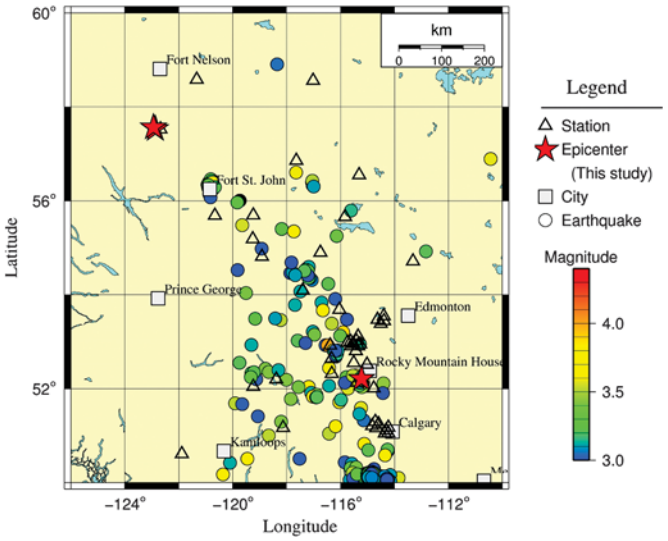

▲ **Figure 1.** Events of **M** >3 (1985–2014) and network stations (2014).

THE STUDY EVENTS AND GROUND MOTIONS

Figure 1 shows the location of the three study events and seismographic stations in relation to the regional seismicity. Table 1 summarizes the event locations and alternative magnitude estimates. The alternative magnitudes include the catalog local magnitudes (M_L) according to the Geological Survey of Canada (GSC), and the moment magnitudes as estimated using three different methods. The moment magnitude estimation methods include the simulation-based algorithm of Atkinson *et al.* (2014), the empirically calibrated regional estimation method of Atkinson and Babaie Mahani (2013), and the regional moment tensor (RMT) solution. We have two alternative RMT solutions for two of the events; one was provided by the GSC (Honn Kao, personal comm., 2014), and we computed the other using software provided by R. Herrmann (St. Louis University). The alternative moment magnitude estimates agree well with each other, yielding our preferred magnitude estimates of **M** 4.0, 4.2, and 3.9 for the 30 July, 4 August, and 9 August events, respectively.

The accuracy of event locations is of particular importance when trying to determine potential causes for an event. Using the approach of Peters and Crosson (1972), it is possible to estimate the expected location error for an event from the station geometry. Based on available stations, we believe the location accuracy is on the order of 5 km for the FSJ events and is approximately 2 km for the RMH event.

The events of **M** 4.0 and 4.2 near FSJ are very likely to have been induced by hydraulic fracturing, based on focal depth, proximity to wells, and information made available in personal communications to the authors. These events occurred at shal-

Table 1
Summary of Event Parameters

Date (yyyy/mm/dd)	Time (UTC) (hh:mm)	Latitude (°)	Longitude (°)	M (AGY14)*	M (AB13)	M (RMT)	M_L (GSC)
2014/07/30	21:23	57.530	−122.870	**4.0**	3.9	3.8	3.8
2014/08/04 2014/08/09	17:17	57.560	−122.940	**4.2**	4.2	4.2 (NMX)–4.4 (GSC)	4.0
2014/08/04 2014/08/09	15:28	52.208	−115.218	**3.9**	3.9	3.8 (GSC)–3.9 (NMX)	4.3

Notes: The three **M** estimates were obtained using the algorithms of Atkinson et al. (2014, AGY14), Atkinson and Babaie Mahani (2013, AB13), and a regional moment tensor (RMT) solution; RMT solutions are from the Geological Survey of Canada (GSC) (H. Kao, personal comm., 2014) and Nanometrics (NMX) (computed by the last author). The local magnitude from the GSC (M_L) is also given.
*Our preferred value of magnitude is given in bold.

low depth (~2–5 km, according to poorly constrained RMT solutions) and were felt to distances of more than 200 km, with maximum reported intensities of IV–V for the larger event. There is one water disposal well in the area, but it is located a significant distance (~12 km) from the epicenters of the 30 July and 4 August events and has not been previously associated with induced events, despite having been in operation since 2009. The cumulative volume injected to date is 136, 874 m^3 (according to information publicly available through information filed with the Alberta Energy Regulator). Monthly water injection volumes at this well were reduced significantly beginning in January 2013, and this, in combination with the distance, greatly reduces the likelihood of injection operations as the trigger for the events in question. Assuming the events were induced, the trigger was most likely related to well stimulation operations that appear to have been in progress at the time of the events. It is possible, however, that a combination of factors was involved (e.g., the slight increase in pore pressure due to the disposal well at distance made the faults near the hydraulic fracture operations more prone to slip).

Multistage hydraulic fracture treatments of horizontal completions have been used to develop natural gas resources in the Triassic Montney Formation in the immediate region of the FSJ events since 2010. The horizontal completions are typically 1500 m long and are stimulated by hydraulic fracture in eight or nine stages. A single stage treatment typically requires 8–12 hr, with average-injected water volumes of ~820 m^3 per stage for nitrified slickwater systems (Johnson and Johnson, 2012). Following the hydraulic fracture treatment, the well moves into production phase (and no further hydraulic fracture stimulation is conducted). Three wells are producing gas from the Montney Formation in the immediate vicinity of the epicenters, and six wells completed drilling prior to the 30 July **M** 4.0 event; a seventh well was being drilled at the time of both events. The perforation and treatment records for the 2014 wells were not available at the time of writing, but there is a high probability that the wells received hydraulic fracture treatments similar to other Montney gas wells in the field, during a time period consistent with the occurrence of the events. The 9 August **M** 3.9 event near RMH, the strongest event to occur in Alberta in more than a decade, is ambiguous in origin. Its focal depth is poorly constrained, with RMT solutions suggesting depths near 4 km but possibly as deep as 8 km. This area experienced induced seismicity in the 1980s that has been associated with volume changes at depth due to gas extraction (Baranova *et al.*, 1999), but this activity has been in decline since the 1990s. Unlike the FSJ area, there are no records of recent oil and gas drilling and stimulation operations in the RMH area. However, two active water disposal wells are located 1700 and 3600 m from the event epicenter (according to information on file with the Alberta Energy Regulator). The closer of the two (KEYSPAN STRACHAN 6-33-37-9W5) was installed in 1971 and has injected a cumulative volume of over 3 M m^3 (19 million barrels) of formation brine into the Devonian Leduc Formation at 4275–4295 m depth; recent injection rates average 120 m^3 per day. Operations in the other disposal well (HUSKY STRACHAN 10-30-37-9W5) began in mid-2013, with a cumulative injection of 110, 000 m^3 (690,000 barrels) into the Devonian Wabamun Formation at 3795–3900 m depths. Injection rates are approximately twice those of the 6-33 well, but the cumulative volume to date is lower.

The **M** 3.9 RMH event was felt strongly by nearby residents, with a maximum reported intensity of IV–V. It caused a power outage that lasted for several hours, because the ground motions were sufficient to trip a substation in the epicentral area (Global News, 2014). A nearby gas plant automatically shut down and flared gas as a precautionary measure, and minor secondary effects were experienced at power plants throughout the region.

We examine the ground motions from these three similar-sized events using high-quality three-component broadband seismographic data from the TransAlta/Nanometrics regional network (TA network), the northeastern British Columbia network of the Pacific Geoscience Center (NBC), the Alberta Geological Survey (AGS), and the Canadian National Seismographic Network (CNSN). (There are no available strong-motion stations in the region.) We processed the time series as described in Assatourians and Atkinson (2010). Briefly, the velocity time series are corrected for glitches and trends, then filtered and corrected for instrument response in the frequency domain. Differentiation to generate acceleration time series is done in the frequency domain before conversion back to the time domain.

Peak ground velocity (PGV) and peak ground acceleration values are found from peak amplitudes of instrument-corrected time series, and pseudospectral accelerations (PSAs, 5% damped) are calculated from the corrected acceleration time series following the Nigam and Jennings (1969) formulation for the computation of response spectra. The results of the processing procedures were validated against other standard processing software, as described in Assatourians and Atkinson (2010).

Figure 2 provides an overview of the vertical-component 1 Hz PSA values from the three events in comparison with the simulation-based ground-motion model of Atkinson *et al.* (2014) (also for the vertical component), from which the moment magnitudes were determined (Table 1). To place the observations in a broader ground-motion context, recorded PSA 1 Hz amplitudes from the Next Generation Attenuation (NGA)-West 2 database in California, for events of similar magnitude, are also shown, along with a recent ground-motion prediction equation (GMPE) developed for such events from this database (Atkinson, 2015, hereafter referred as A15). Note that the distance metric for all observations, and for the plotted GMPEs, is hypocentral distance. It is apparent that the recorded motions are generally consistent with expected amplitudes for events of similar size in California.

The NGA-West 2 data and the A15 GMPE are actually for the geometric-mean horizontal component but both are corrected to a reference boundary site condition of B/C (V_{S30} = 760 m/s, in which V_{S30} is the time-averaged shear-wave velocity over the top 30 m), using site-amplification factors that were derived from the NGA-West 2 database (see Boore *et al.*, 2014). This correction to the B/C site condition removes much of the site amplification effects that cause the horizontal-component amplitudes to exceed those of the vertical component. Thus, the site-corrected horizontal motions can be reasonably compared with vertical-component motions as a first approximation. Such an approximation neglects a modest amplification that would be expected on firm sites (B/C) on the horizontal component, relative to the vertical, due to travel through the crustal velocity gradient. As discussed by Atkinson and Boore (2006), we would expect this factor to be approximately unity at low frequencies and to increase gradually with frequency to a value near 2 for high frequencies, with the details of this function depending on the velocity profile and the near-surface kappa (attenuation). We do not attempt to make any correction for this in the comparison plots in Figure 2, because we expect the horizontal-to-vertical (H/V) ratio at most sites should be near unity at 1 Hz based on preliminary evaluations, and thus Figure 2 is relatively unaffected by this issue. A detailed study of site amplification characteristics at these stations is underway and will be the subject of a future paper.

In Figure 3, we compare the horizontal-component motions (both components are plotted) for all three events, in comparison with the A15 GMPE. We converted the A15 predictions for B/C site conditions to equivalent values for National Earthquake Hazards Reduction Program (NEHRP) D sites with V_{S30} from 250 to 300 m/s range, assuming the site

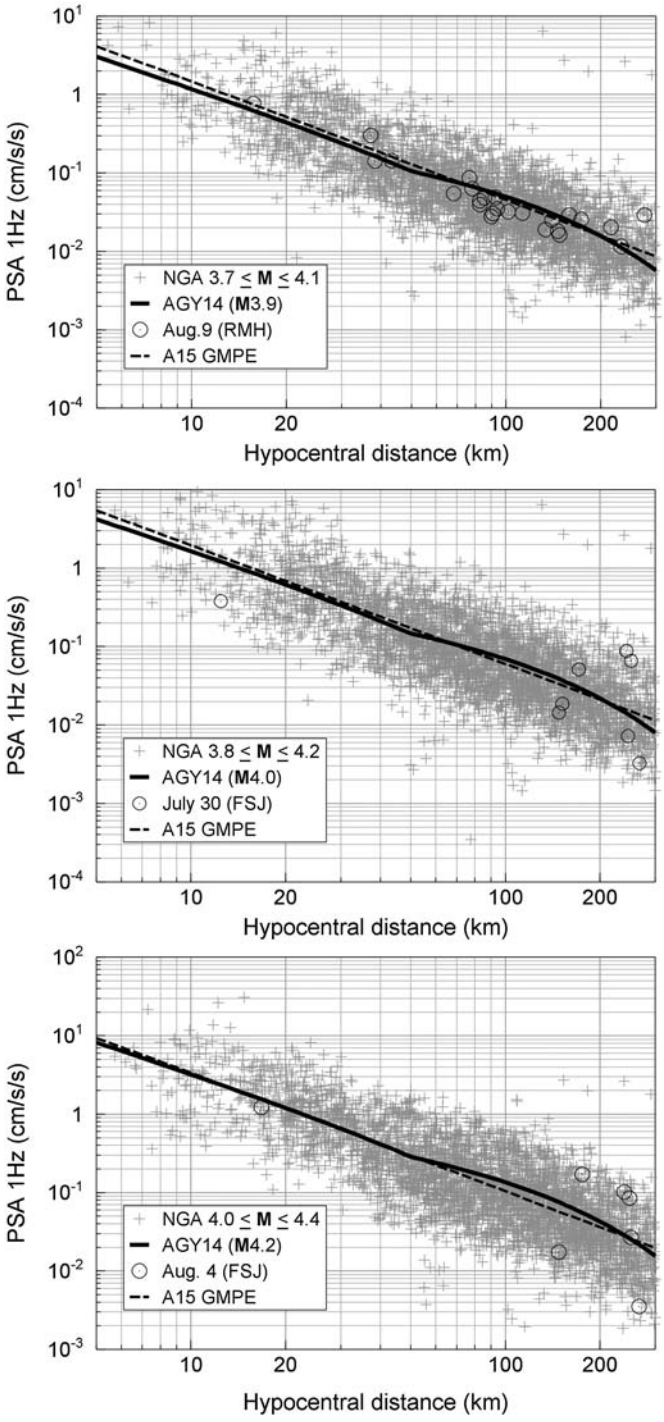

▲ **Figure 2.** 1 Hz pseudospectral acceleration (PSA) (vertical component) for three study events (circles) in comparison with the Atkinson *et al.* (2014) vertical-component magnitude scaling curve (AGY14, solid line) from which moment magnitude is determined. The dashed line shows the ground-motion prediction equation (GMPE) of Atkinson (2015) (horizontal component on B/C site conditions). The light plus symbols show California data from the Next Generation Attenuation (NGA)-West 2 database (horizontal components, corrected to B/C site conditions) for events in same magnitude range (±0.2 units).

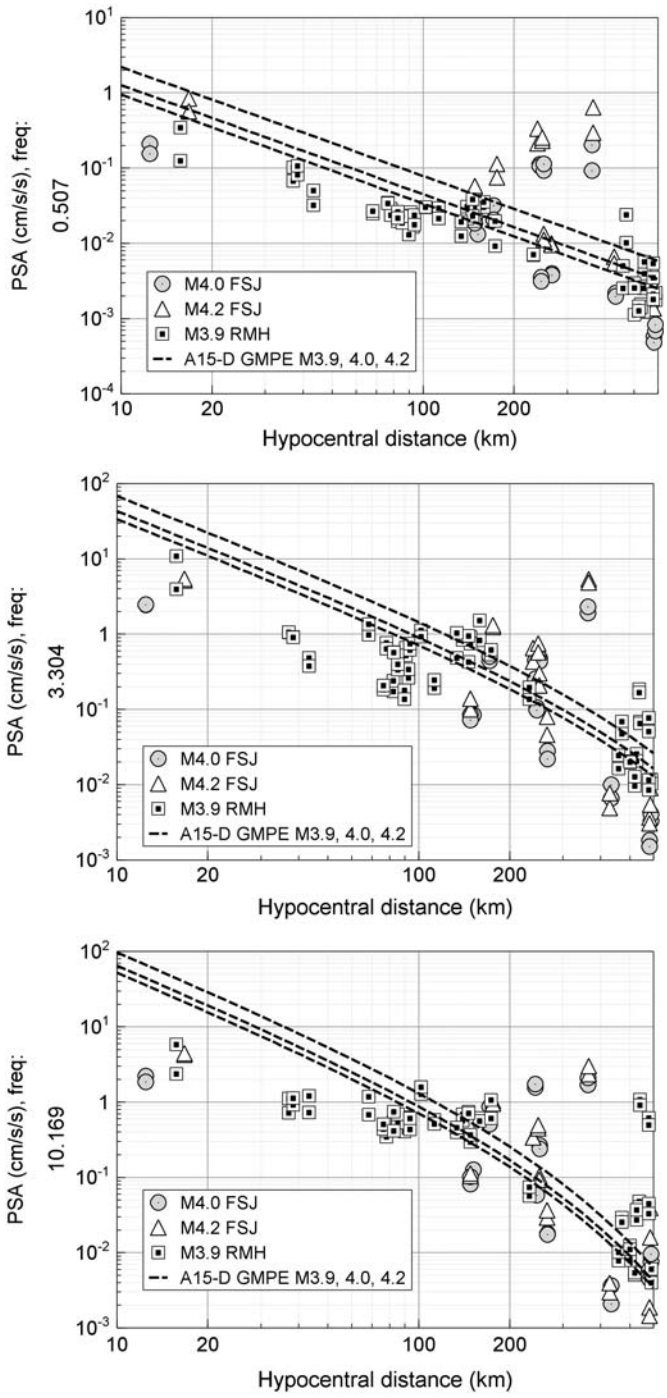

▲ **Figure 3.** Horizontal-component PSA for frequencies of (top) 0.5, (middle) 3.3, and (bottom) 10 Hz for the three study events (**M** 4.0 and **M** 4.2 near Fort St. John [FSJ], **M** 3.9 near RHM), in comparison with the A15 GMPE (D site conditions) for the corresponding magnitudes. The assumed site amplification factors for the A15 GMPE, to convert from B/C to D site conditions, are 3.1, 2.2, and 1.6 for frequencies 0.5, 3.3, and 10 Hz, respectively.

amplification model of Boore *et al.* (2014). The assumption of site class D as an average condition reflects our limited knowledge of the sites—we believe most of them to be situated on soil, ranging from soft to firm, but investigations of the site response characteristics are ongoing. The instruments in the TA network from which most of the data are derived are posthole seismometers, which are driven to a depth of firm resistance, typically a few meters. A generic description of "firm soil" might thus apply to most of these sites. We assume linear site amplification, though we recognize that at close distances the motions may have been strong enough to cause some minor nonlinearity in response. The resulting amplification factors applied to the A15 GMPE are 3.1, 2.2, and 1.5 for frequencies of 0.5, 3.3, and 10 Hz, respectively.

Based on inspection of Figure 3, there are several sites, located at 200–400 km distances from the FSJ events, that may have very significant site amplification, especially at lower frequencies (the very high amplitude points). These are the northernmost NBC stations and the CNSN HILA station. For these stations, the horizontal ground motions are significantly larger than predicted by the A15 GMPE. At distances less than 100 km, the motions tend to be lower than those predicted by the A15 GMPE, especially at high frequencies, if we assume D soil conditions on average. This could reflect stress drops that are lower than the average implied by the A15 model and/or possibly lower levels of site response than those assumed. Resolution of this issue will require further studies of both event and site characteristics.

To investigate whether a low stress drop may be responsible for the relatively low 10 Hz amplitudes of ground motion seen at <100 km in Figure 3, the response spectra are examined as a function of frequency using nearby records only (Fig. 4). For each event, the closest station is in the 12 to 18 km hypocentral distance range. We compare the observed spectra with the A15 empirical GMPE model for California. We show both the horizontal and vertical components in this plot to provide some insight into the possible influence of site effects. Note that the A15 model spectrum might be expected to agree more closely with the vertical than the horizontal components, because the A15 model is for B/C site conditions and thus represents only a modest level of site amplification. We also compare the spectra ewith a calibrated simulation model for **M** 4 events in California; the simulation model was developed by Yenier and Atkinson (2014, hereafter referred as the YA14 model) using an equivalent point-source stochastic model, for which parameters were calibrated against the NGA-West 2 database. Based on the consistently low amplitudes at $f > 2$ Hz relative to the A15 or YA14 models as seen in Figure 4, we infer that these three events had a significantly lower stress drop than is typical for natural events in California of similar magnitude. Even if we assume the observed horizontal components were not amplified relative to the model expectations for B/C site conditions, we would still conclude the high-frequency amplitudes are low relative to those predicted. However, this conclusion is based only on examination of the spectra from the closest station, which may not be representative of the overall source properties of the events.

To check if our inference regarding the low stress drop of the three events is robust, we take all vertical-component spectra

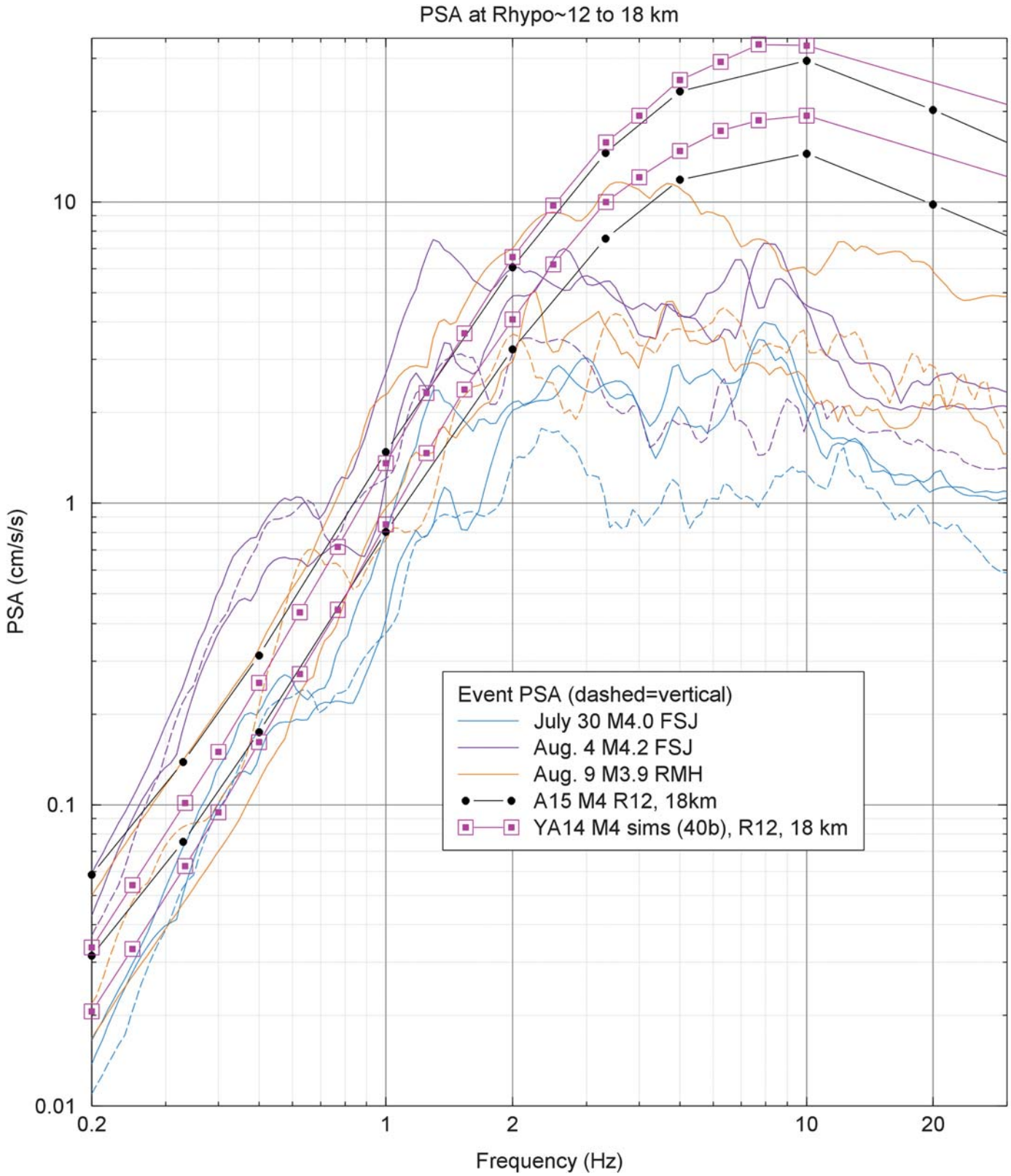

▲ **Figure 4.** PSA (5% damped; solid lines horizontal component, dashed lines vertical component) at closest station to each of the three events (R_{hypo} = 12–18 km), in comparison with the A15 GMPE spectrum for **M** 4 at 12–18 km and the Yenier and Atkinson (2014) western North America simulation model for **M** 4 at 12–18 km.

for each event within 300 km, to provide a larger set of records, and correct them to an equivalent hypocentral distance of 10 km using the A15 attenuation model (i.e., the attenuation curve plotted in Fig. 2). We use the vertical component to minimize the influence of site response. The average of the distance-corrected spectra gives us a more robust estimate of the near-source spectrum than can be obtained from a single station. Figure 5 shows the apparent source spectra in comparison to the A15 empirical GMPE spectrum and the YA14 simulation model spectrum (both for **M** 4 and at 10 km). Because both the A15 and YA14 models are for the horizontal component (B/C sites), we convert them to the equivalent model spectra for the vertical component by dividing by the expected amplification on the horizontal component for B/C site conditions, following the crustal-amplification model of Atkinson and Boore (2006). Thus, the model spectra correspond to the vertical component for B/C site conditions. To be consistent with the plotting of the vertical-component model spectra for B/C site conditions, we also made a correction to the observed vertical-component spectra, such that they will also apply to B/C site conditions; this implicitly assumes that although site response is less on the vertical than on the horizontal component, it is not entirely absent. For this correction, we use the site amplification model of Stewart *et al.* (2015) for the vertical component. We assume an average site condition for the stations of NEHRP D, with V_{S30} in the 250–300 m/s range. Therefore, we divide the vertical-component spectrum inferred for each event by the vertical-component amplification for D relative to B/C (from Stewart *et al.*, 2015); this is a factor that ranges from about 1.8 at low frequencies to about 1.3 at high frequencies.

In Figure 5, the inferred source spectra of the events appear to be close (within a factor of ~1.5) to those predicted by the model spectra. This suggests the ground motions were comparable with those for events of similar size in the NGA-West 2 database. There is some evidence that the **M** 3.9 RMH event is slightly enriched in high frequencies relative to low frequencies in comparison with the two FSJ events. This indicates a somewhat higher stress drop for the RMH event. Note the predominant microseismic noise peak near 0.3 Hz for the FSJ events, which contaminates the source spectrum at low frequencies and may have led to elevated amplitudes over a broad frequency range.

Considering all three inferred event spectra at $R_{hypo} = 10$ km, the high-frequency amplitudes appear to have similar spectral shapes and high-frequency amplitudes to those predicted for typical California events, on average. We should note the standard error of the estimated source spectrum is very high for the two FSJ events (factor of 4) due to the sparse observations and their large variability. The source spectrum for the RMH event is better determined, with amplitudes having a standard error of about a factor of 2. (Standard errors are not plotted, to avoid cluttering the figure.)

On balance, Figure 5 suggests the stress drops for the three events are in reasonable agreement with values expected for California earthquakes of this size. This conclusion is in contrast to that reached from examination of Figure 4, in which we considered just the nearest stations. The reason for this discrepancy is apparent from inspection of Figure 3: in general, the motions from these events appear to be low relative to predictions for short distances but agree well with model predictions at regional distances. Thus, the stress drop of these events is not well resolved, and our conclusions depend on the relative weight that we accord to the sparse data at close distances. More definitive conclusions on stress drops will require additional datasets with richer close-distance recordings.

We might expect these events to have low stress drops due to their shallow focal depths. A recent study by Yenier and Atkinson (2015a) shows that stress drop is a function of focal depth, with the dependence of stress on focal depth being strongest for small events; moreover, the relationship between stress and depth as obtained from natural earthquakes appears to explain the typical stress drops obtained from induced events in the central United States (Yenier and Atkinson, 2015b). Additional studies of ground-motion data from induced events are needed to corroborate these findings, but we currently believe that induced events have lower stress drops on average than do natural events, due to their shallower-than-average focal depths. We note that Hough (2014) has also suggested that induced events may have low stress drops, based on an analysis of intensity observations from induced versus natural events.

Figures 6 and 7 provide an aerial perspective on the ground motions, in the form of maps that contour the intensity of the motions for the 4 August FSJ and 9 August RMH events. These maps are based on inferred intensities from predicted and recorded PGV and from felt reports made to the GSC through their online reporting tool (which is based on the "Did You Feel It" survey of Wald *et al.*, 1999); events were felt to distances of ~200 km. A coarse grid is first defined over the map area at the integer latitude–longitude points. For each grid point, PGV is calculated using the empirical GMPE of Atkinson (2015) developed for small-to-moderate events, for the event **M** and hypocentral distance. At seismographic sites (exact coordinates), PGV is calculated from the geometrical mean of the three PGV components. Then intensities associated with these two sets of PGV values are calculated following the Worden *et al.* (2012) equations, including the terms in magnitude and distance (equation 6 in Worden *et al.*). These intensities are merged with the felt intensity reports (at their exact coordinates) to form the revised (unevenly spaced) grid of intensity points. Interpolation of these intensities over the map area is based on fitting minimum-curvature surfaces that pass through all tabulated intensity points following Smith and Wessel (1990) (no weighting of the points is performed). The patch of higher observed horizontal-component motions in northern British Columbia that was noted in Figure 3 can be clearly seen in the intensity distribution, as can the influence of the felt intensity points.

SUMMARY AND CONCLUSIONS

We presented an overview of the ground motions recorded during three recent of events of **M** ~ 4 in western Alberta and northeastern British Columbia. The events near FSJ are believed

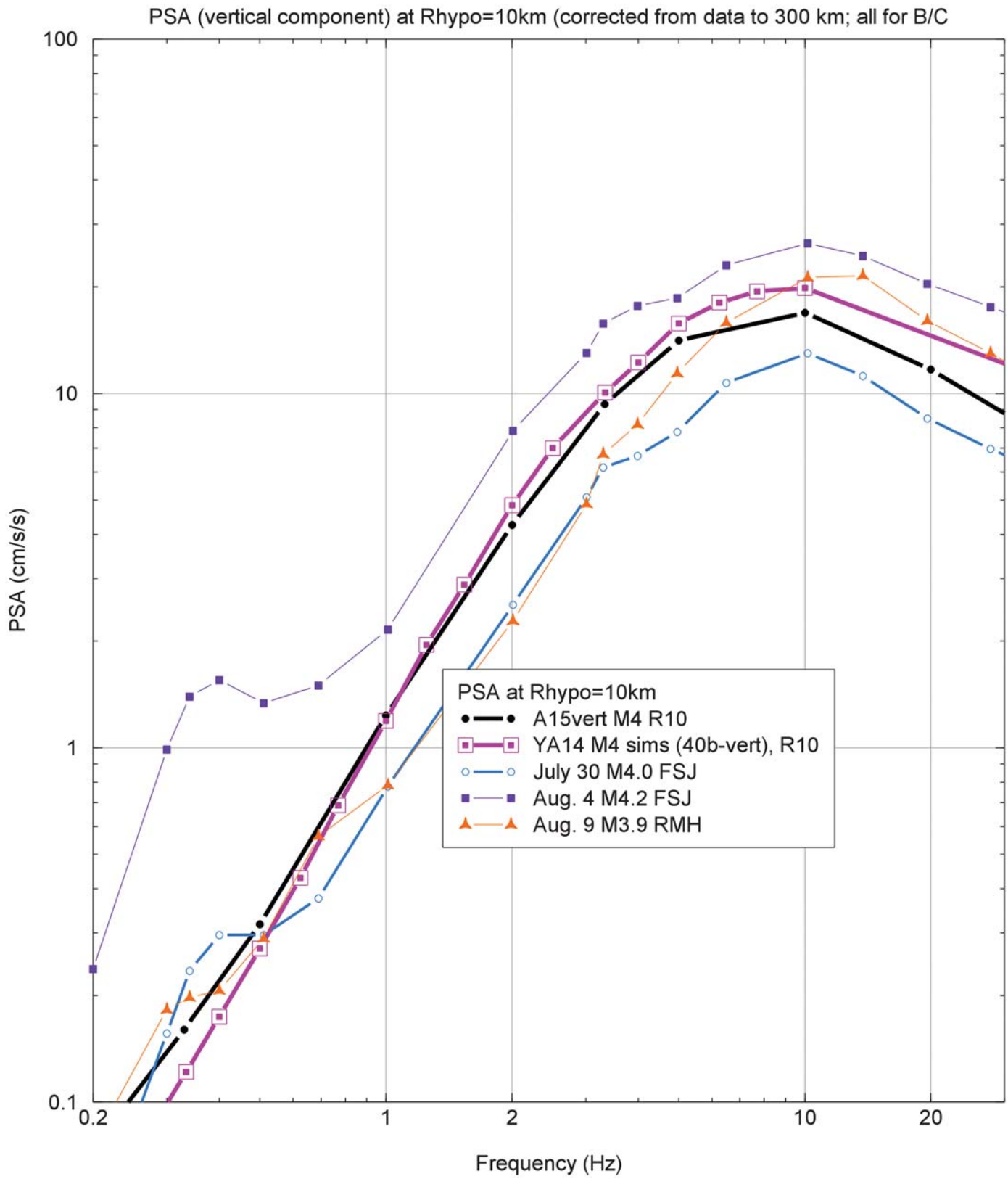

▲ **Figure 5.** Inferred near-source spectra at R_{hypo} = 10 km for the three study events, as computed from vertical-component PSA at <300 km, corrected to 10 km with the A15 attenuation model. The California simulation model spectrum at 10 km for **M** 4 (YA14 model, Yenier and Atkinson, 2014) (inset squares) and empirical GMPE spectrum (A15) model of Atkinson (2015) for **M** 4 at 10 km (solid black circles) are also shown; model spectra have been converted to equivalent vertical spectra, assuming the horizontal-to-vertical model for B/C site conditions as given in Atkinson and Boore (2006). Inferred source spectra for the three events are also corrected to equivalent values for B/C.

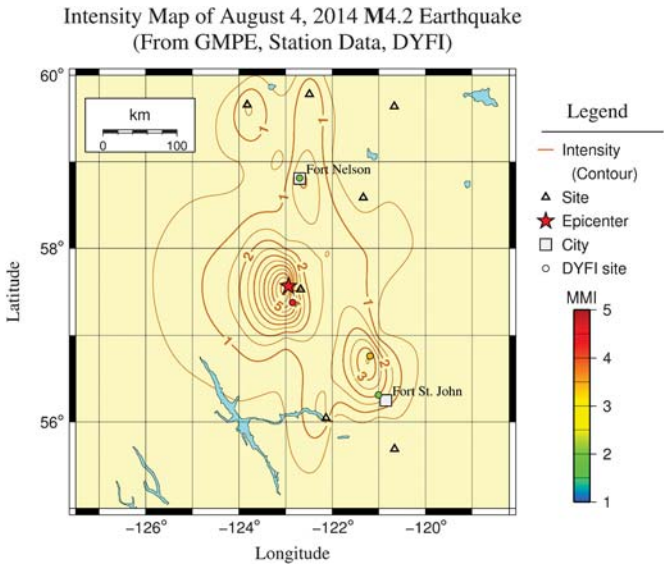

▲ **Figure 6.** Instrumental intensity distribution for the 4 August **M** 4.2 event near FSJ. Maximum predicted instrumental intensity at the epicenter is >6; the felt distance is ~200 km. (DYFI, "Did You Feel It" survey of Wald *et al.*, 1999.)

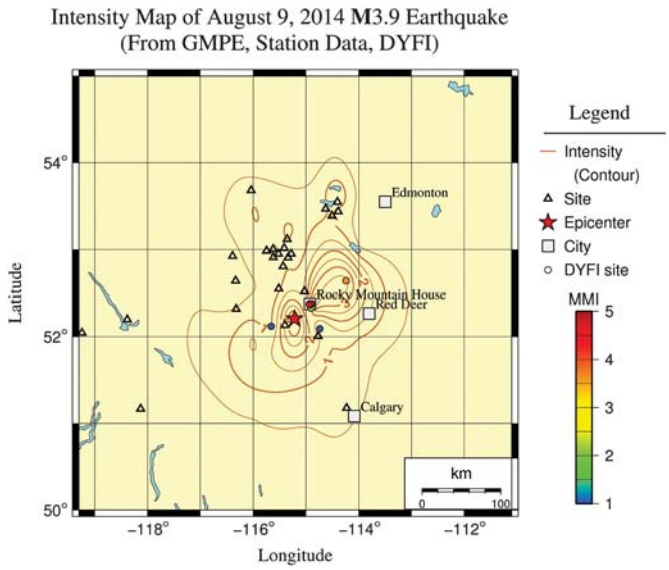

▲ **Figure 7.** Instrumental intensity distribution for the 9 August **M** 3.9 event near Rocky Mountain House (RMH). Maximum reported intensities were 4–5. The felt distance is >100 km. (DYFI, "Did You Feel It" survey of Wald *et al.*, 1999.)

to have been induced by hydraulic fracture treatments and include one of the largest hydraulic-fracturing-induced event to date in the world, to our knowledge (**M** 4.2–4.4). A second apparent M_L 4.4 event was initiated by hydraulic fracturing near Fox Creek, Alberta, on 23 January 2015, as this article was going to press. The **M** 3.9 event near RMH is enigmatic in origin; it may have been induced by wastewater injection or gas extraction, or it may be natural. All three events were widely felt and had the potential to affect infrastructure, if located in close proximity. The largest of the events appeared to produce potentially damaging motions as indicated by predicted epicentral intensities of approximately VI. The smallest of the events produced ground motions large enough to trip a nearby transformer and cause a power outage, illustrating the potential of even small events to cause significant ground motion.

The ground-motion amplitudes from these three events are in reasonable accord with predicted amplitudes for events in California of a similar size, as given by empirical models for small-to-moderate events (Atkinson, 2015) or by simulation-based models (Yenier and Atkinson, 2014). There is some evidence, in the form of relatively low high-frequency amplitudes on the closest stations, for lower-than-average stress drops for these events in comparison with events of similar size in California. This evidence is not clear-cut, because if we consider stations at regional distances, we reach a different conclusion. We believe that induced events may tend to have lower stress drops on average than natural events due to a focal depth effect. Recent evidence shows that stress drop depends on focal depth, especially for small-to-moderate earthquakes (Yenier and Atkinson, 2015a). Further study of ground motions from induced events is required to better document the range of motions that can be expected at close distances and their damage potential. Our preliminary findings suggest that moderate-induced events (**M** 4–5) may be damaging to nearby infrastructure, because the shallow focal depth brings the earthquake source very close to surface facilities located within a small radius of the epicenter. This may result in localized strong ground motions, to which some infrastructure may be vulnerable—particularly in low-to-moderate seismicity regions, where seismic resistance of infrastructure may be limited. However, a mitigating factor is that the shallow depth may result in low stress drops on average, thereby limiting high-frequency motions. More detailed studies of the interaction between factors controlling the ground motions and their damage potential requires improved seismographic monitoring with broadband three-component sensors in the immediate vicinity of both hydraulic fracture and fluid injection sites, and strong-motion monitoring of nearby infrastructure.

ACKNOWLEDGMENTS

Funding by TransAlta for the seismographic network and research program is gratefully acknowledged. The research program is also supported by the Natural Sciences and Engineering Research Council of Canada. We thank Stephen Halchuk of the Geological Survey of Canada for providing felt intensity data and Honn Kao for providing preliminary regional moment tensor solutions. We are grateful to two anonymous referees for their helpful comments which resulted in an improved article.

REFERENCES

Assatourians, K., and G. Atkinson (2010). Database of processed time series and response spectra for Canada: An example application

to study of the 2005 M_N 5.4 Riviere du Loup, Quebec earthquake, *Seismol. Res. Lett.* **81,** 1013–1031.

Atkinson, G. (2015). Ground-motion prediction equation for small-to-moderate events at short hypocentral distances, with application to induced seismicity hazards, *Bull. Seismol. Soc. Am.* **105,** no. 2A, doi: 10.1785/0120140142.

Atkinson, G., and A. Babaie Mahani (2013). Estimation of moment magnitude from ground motions at regional distances, *Bull. Seismol. Soc. Am.* **103,** 107–116.

Atkinson, G., and D. Boore (2006). Ground motion prediction equations for earthquakes in eastern North America, *Bull. Seismol. Soc. Am.* **96,** 2181–2205.

Atkinson, G., H. Ghofrani, and K. Assatourians (2015). Impact of induced seismicity on the evaluation of seismic hazard: Some preliminary considerations, *Seismol. Res. Lett.* **86,** no. 3, doi: 10.1785/0220140204.

Atkinson, G., D. W. Greig, and E. Yenier (2014). Estimation of moment magnitude (M) for small events (M < 4) on local networks, *Seismol. Res. Lett.* **85,** 1116–1124.

Baranova, V., A. Mustaqeem, and S. Bell (1999). A model for induced seismicity caused by hydrocarbon production in the western Canada sedimentary basin, *Can. J. Earth Sci.* **36,** 47–64.

B.C. Oil and Gas Commission (2012). *Investigation of Observed Seismicity in the Horn River Basin*, Victoria, British Columbia, 29 pp., www.bcogc.ca (last accessed December 2014).

Boore, D., J. Stewart, E. Seyhan, and G. Atkinson (2014). NGA-West2 equations for predicting response spectral accelerations for shallow crustal earthquakes, *Earthq. Spectra* **30,** 1057–1086.

Ellsworth, W. (2013). Injection-induced earthquakes, *Science* **341,** no. 6142, doi: 10.1126/science.1225942.

Global News (2014). Earthquake hits northeast of Rocky Mountain House, http://globalnews.ca/news/1501147/earthquake-hits-northeast-of-rocky-mountain-house-power-outages-reported/ (last accessed December 2014).

Hassani, B., and G. Atkinson (2015). Referenced empirical ground-motion model for eastern North America, *Seismol. Res. Lett.* **86,** no. 2A, 477–491, doi: 10.1785/0220140156.

Hough, S. (2014). Shaking from injection-induced earthquakes in the central and eastern United States, *Bull. Seismol. Soc. Am.* **104,** no. 5, 2619, doi: 10.1785/0120140099.

Johnson, E., and L. Johnson (2012). Hydraulic fracture water usage in northeast British Columbia: Locations, volumes and trends, in *Geoscience Reports 2012*, British Columbia Ministry of Energy and Mines, Victoria, British Columbia, 41–63.

Keranen, K., H. Savage, G. Abers, and E. Cochran (2013). Potential induced earthquakes in Oklahoma, USA: Links between wastewater injection and the 2011 M_w 5.7 earthquake sequence, *Geology* **41,** no. 6, 699, doi: 10.1130/G34045.1.

Nigam, N. C., and P. C. Jennings (1969). Calculation of response spectra from strong motion earthquake records, *Bull. Seismol. Soc. Am.* **59,** 909–922.

Novakovic, M., G. Atkinson, and B. Cheadle (2014). Investigation of seismicity in the Crooked Lake region of Alberta, presented at *CGU Annual Meeting*, Banff, Alberta, 5–7 May 2014.

Peters, D., and R. Crosson (1972). Application of prediction analysis to hypocenter determination using a local array, *Bull. Seismol. Soc. Am.* **62,** 775–788.

Smith, W. H. F., and P. Wessel (1990). Gridding with continuous curvature splines in tension, *Geophysics* **55,** 293–305.

Stewart, J., D. Boore, E. Seyhan, and G. Atkinson (2015). NGA-West2 equations for predicting vertical-component PGA, PGV, and 5%-damped PSA from shallow crustal earthquakes, *Earthq. Spectra*, in press.

Sumy, D., E. Cochran, K. Keranen, M. Wei, and G. Abers (2014). Observations of static Coulomb stress triggering of the November 2011 M 5.7 Oklahoma earthquake sequence, *J. Geophys. Res.* **119,** 1904–1923, doi: 10.1002/2013JB010612.

U.S. National Research Council (2012). *Induced Seismicity Potential in Energy Technologies*, 300 pp., http://www.nap.edu/catalog.php?record_id=13355 (last accessed December 2014), ISBN: 978-0-309-25367-3.

Wald, D., V. Quitoriano, L. Dengler, and J. Dewey (1999). Utilization of the Internet for rapid community intensity maps, *Seismol. Res. Lett.* **70,** 680–697.

Worden, B., M. Gerstenberger, D. Rhoades, and D. Wald (2012). Probabilistic relationships between ground motion parameters and modified Mercalli intensity in California, *Bull. Seismol. Soc. Am.* **102,** 204–221.

Yenier, E., and G. Atkinson (2014). Point-source modeling of moderate-to-large magnitude earthquakes and associated ground-motion saturation effects, *Bull. Seismol. Soc. Am.* **104,** no. 3, 1458, doi: 10.1785/0120130147.

Yenier, E., and G. Atkinson (2015a). An equivalent point-source model for stochastic simulation of earthquake ground motions in California, *Bull. Seismol. Soc. Am.* **105,** no. 3 (in press).

Yenier, E., and G. Atkinson (2015b). A regionally-adjustable generic GMPE based on stochastic point-source simulations, *Bull. Seismol. Soc. Am.*, submitted.

Gail Atkinson
Karen Assatourians
Burns Cheadle
Western University
London, Ontario
Canada N6A 5B7
gmatkinson@aol.com

Wes Greig
Nanometrics Inc.
250 Herzberg Road
Kanata, Ontario
Canada K2K 2A1

Published Online 1 April 2015